Martian high latitude permafrost depth and surface cover thermal inertia distributions

Joshua L. Bandfield[1] and William C. Feldman[2]

[1] Martian high latitudes have thermal properties consistent with an extensive high thermal inertia permafrost layer near the surface. Surface cover thermal inertias and permafrost depths at Martian high latitudes ($50°–80°$N/S) are derived from Thermal Emission Spectrometer (TES) data and compared with previously published water ice depths determined from the Mars Odyssey Neutron Spectrometer (MONS). The depth to the permafrost layer is correlated with surface cover thermal inertia, albedo, and latitude in general agreement with predicted trends of water ice stability. Comparison of permafrost depths with water ice rich layer depths derived from MONS data displays good qualitative agreement, although a divergence is present at greater burial depths. This disparity may be due to the presence of hydrated minerals at shallow depths or a lower than expected permafrost thermal inertia corresponding with low water ice concentrations at greater depths. Surface cover thermal inertias are greater in the northern high latitudes than in the south and differences between these and previous results will have significant effects on the predicted depth of Martian water ice stability. Several regions in the northern hemisphere display high surface cover thermal inertia associated with possible receding water ice deposits that are shallow enough to influence diurnal surface temperatures. Significant lateral and vertical heterogeneity in water ice distributions are present and the Martian regolith is likely more complicated than can be described by simple two layered models and a single mode of water ice emplacement.

Citation: Bandfield, J. L., and W. C. Feldman (2008), Martian high latitude permafrost depth and surface cover thermal inertia distributions, *J. Geophys. Res.*, *113*, E08001, doi:10.1029/2007JE003007.

1. Introduction

[2] The high concentrations of water ice inferred from Gamma Ray Spectrometer suite of measurements [*Boynton et al.*, 2002; *Feldman et al.*, 2004; *Mitrofanov et al.*, 2004] are consistent with a high concentration of water ice in the shallow subsurface on Mars. Measurements of thermal, epithermal, and fast neutron leakage currents are sensitive to the abundance of hydrogen. Differences in sensitivity and penetration depth between these measurements provide the ability to determine water equivalent hydrogen (WEH) abundance and depth to a water-rich layer using a simple two-layered model [e.g., *Feldman et al.*, 2007].

[3] Martian high latitudes also have thermal properties consistent with an extensive high thermal inertia layer within a few centimeters of the surface. This subsurface water-ice/regolith mixture will have a thermal inertia similar to solid bedrock that is much higher than the more porous dry particulate regolith cover [*Paige*, 1992; *Mellon et al.*, 2004; *Schorghofer and Aharonson*, 2005; *Titus et al.*, 2003; *Bandfield*, 2007]. Several studies have taken advantage of

these properties to determine the structure of the near-surface within high latitude localities [*Titus et al.*, 2003; *Armstrong et al.*, 2005; *Bandfield*, 2007].

[4] The neutron and temperature results are largely in agreement with models of theoretical water-ice stability [e.g., *Leighton and Murray*, 1966; *Fanale et al.*, 1986; *Zent et al.*, 1986; *Mellon and Jakosky*, 1995; *Mellon et al.*, 2004; *Schorghofer and Aharonson*, 2005]. Vapor diffusion models predict a water-ice table that generally increases in depth with decreasing latitude. More detailed modeling shows that the depth of stability can be highly variable, owing to local surface heterogeneities such as rocks and slopes, and the thermal inertia of the ground cover [*Sizemore and Mellon*, 2006; *Aharonson and Schorghofer*, 2006]. However, despite the broad agreement, significant differences are present between these models [*Diez et al.*, 2008] and several regions display significant differences between predicted water ice depths derived from the models and the neutron and temperature data sets [*Bandfield*, 2007; *Diez et al.*, 2008].

[5] In this manuscript, we derive surface cover thermal inertias and permafrost depths at Martian high latitudes from Thermal Emission Spectrometer (TES) data and compare the results with previously published water ice depths determined from the Mars Odyssey Neutron Spectrometer (MONS [*Feldman et al.*, 2007]). This comparison provides confirmation of the Neutron Spectrometer results using completely independent measurements and models. In

[1]Department of Earth and Space Sciences, University of Washington, Seattle, Washington, USA.
[2]Planetary Science Institute, Tucson, Arizona, USA.

addition, the two techniques have different sensitivities that allow for inferences to be made regarding the nature of Martian high latitude water ice deposits. Each data set contains details and sensitivities that can also help describe the current Martian water cycle and its relationship to local conditions and global climate cycles.

2. Data Sets and Method

[6] Both surface temperature and neutron flux measurements require simplifying assumptions in order to model a complex system using relatively simple data sets. In the case of the neutron measurements, it is assumed that the hydrogen detected is in the form of water. For comparison with the ice depths determined from the TES data, it is assumed that the water is in the form of ice. The analyses of the surface temperatures assume that any buried high thermal inertia layer is a solid mixture of regolith and ice with a thermal inertia of 2290 J m^{-2} K^{-1} s$^{-0.5}$, (MKS units are used for thermal inertia throughout this manuscript). For the purpose of this paper, we use the term "permafrost" to describe a buried high inertia surface detected using temperature measurements and "water ice" to describe the high latitude hydrogen concentrations detected using neutron measurements. Both techniques must infer the presence of water ice based on what are widely considered reasonable assumptions of the characteristics of Martian high latitude surfaces.

[7] In addition, both models assume a relatively simple two layered geometry of relatively dry soil cover on top of a semi-infinite water rich layer that is assumed constant throughout the measurement field of view. Clearly, more complicated systems are likely to be common on Mars, but the data sets do not have the leverage to converge on a unique solution based on more complex geometries.

2.1. TES Instrument and Data

[8] The TES instrument is a Fourier transform Michelson interferometer ($\sim$6–50 μm) with co-aligned thermal (5–100 μm) and visible (0.3–3 μm) bolometers. The detectors are arranged in a 3 by 2 array, each with an 8 mrad instantaneous field of view with a 1.8 s integration time. This configuration results in a 3 by $\sim$8 km footprint from the $\sim$380 km MGS mapping orbit with the elongation due to smear from the lack of image motion compensation. A pointing mirror allows for along track targeting capability as well as viewing of the limb, space, and an internal reference surface. Details of instrument calibration and observations are described by *Christensen et al.* [2001].

[9] This study utilizes the estimated surface kinetic temperature (target_temp in the TES data set) derived from spectral, rather than bolometer, measurements because they are less susceptible to atmospheric effects. Observations were restricted to emission angles less than 30°, 50°–80° latitude (north and south), and 0100–0300 local time. The data were averaged in bins of 2° latitude, 4° longitude and 4.5° L$_s$. Each bin contained an average of $\sim$90 observations although there was a considerable variation in the actual number of observations within each bin.

2.2. Thermal Model Description

[10] The temperature of any given surface can be predicted using a thermal model and input parameters (e.g.,

latitude, season, elevation, local time, albedo, atmospheric dust opacity, thermal inertia, slope, and azimuth). We use the KRC thermal model (*H.H. Kieffer*, Thermal models for analysis of Mars infrared mapping, manuscript in preparation) to predict surface temperatures. This model has been used by a number of researchers [e.g., *Titus et al.*, 2003; *Fergason et al.*, 2006; *Bandfield*, 2007; *Bandfield and Edwards*, 2008] and allows for customization of a wide variety of parameters such as changes in subsurface thermophysical properties and atmospheric aerosol properties. Results compare favorably with a related thermal model [*Fergason et al.*, 2006] that has been used to derive surface thermal inertias from TES data [*Jakosky et al.*, 2000; *Mellon et al.*, 2000; *Putzig et al.*, 2005]. The parameters used for the surface temperature modeling are listed in Table 1.

[11] Thermal inertias derived from measurements with low angles of solar incidence are not as accurate as those derived from nighttime temperature measurements because of the dominant influence of slope, albedo, and atmospheric aerosol characteristics and their associated uncertainties (see discussion in section 2.5 below). For this reason, we avoided descending orbit observations at local times of 1300–1500. The model was set to run for two Martian years before outputting surface temperatures for the third year. The effects of uncertainties in the thermal modeling will be discussed in the uncertainties section below.

2.3. Application of Thermal Model to TES Data

[12] Each latitude/longitude bin of seasonal surface temperature data was fit individually using a nonlinear least squares fitting routine. All modeling parameters were fixed except surface cover thermal inertia and depth of the permafrost layer. The seasons used for fitting were restricted to summer and early fall seasons (L$_s$ 85.5–220.5 and 265.5–40.5 for the northern and southern hemispheres respectively). In addition, all surface temperatures below 160K were not used for fitting because of the proximity to CO$_2$ condensation temperatures. These restrictions as well as the use of only 0100–0300 local time data isolated the model and data from conditions of significant modeling uncertainty, such as low solar incidence or CO$_2$ frost conditions [e.g., *Bandfield*, 2007].

[13] Top layer inertias were allowed to vary from 60–800, corresponding to diurnal skin depths of $\sim$0.3 to 11 cm. Values below this range pose numerical stability problems with the thermal model and values above this range do not provide enough contrast from the permafrost layer to be distinguished. The model permafrost layer has fixed thermophysical properties (Table 1), but was allowed to vary from 1.15 to 20.3 diurnal skin depths. Shallower depths have a significant influence on the diurnal temperature cycle and are not distinguishable from a higher surface cover thermal inertia. Greater depths have little influence on the seasonal temperature cycle and are not detectable. As a result, the model and fitting routine is sensitive to permafrost at 0.3–6 and 12–220 cm depths for surface cover thermal inertias of 60 and 800 respectively. Water ice and solid rock have similar thermal inertias (primarily because of offsetting heat capacity and density values) and it is not possible to determine the concentration of water in the permafrost layer solely from the temperature data used here.

Table 1. Parameters for the Thermal Model Used in This Study

Parameter	Value
Albedo	Derived from local daytime measurements, 0.65 if frost covered
First layer thickness	0.20 times local skin depth
Succeeding layer thickness	1.15 times preceding layer scaled to local skin depth
Soil cover thermal inertia range	$60-800$ J m^{-2} K^{-1} s$^{-1/2}$
Permafrost depth range	$1.15-20.3$ diurnal skin depths
Soil cover density	1500 kg m^{-3}
Soil cover heat capacity	837 J kg^{-1} K^{-1}
Permafrost density	2018 kg m^{-3}
Permafrost heat capacity	1040 J kg^{-1} K^{-1}
Permafrost thermal conductivity	2.5 W m^{-1} K^{-1}
Visible wavelength dust opacity	0.3
Dust single scattering albedo	0.90
Dust asymmetry scattering parameter	0.50

2.4. Neutron Spectrometer Instrument and Data

[14] The Mars Odyssey Neutron Spectrometer (MONS) sensor assembly is a 10 cm cube of borated plastic scintillator that is split into four, optically isolated prisms, each viewed separately by a photomultiplier tube [*Feldman et al.*, 2002; *Boynton et al.*, 2004]. The cube is cantilevered from the top deck of the Mars Odyssey spacecraft with a free field of view of Mars. One of the prisms (Prism 1) is always facing downward to Mars and is well shielded from the spacecraft by the other three prisms. It is also covered by 0.68-mm-thick sheets of Cd to shield it from thermal neutrons coming from Mars and the spacecraft. Two other prisms view at right angles to the nadir such that one (Prism 2) always views along the spacecraft velocity vector and one (Prism 4) views in the opposite direction. The fact that the spacecraft travels at a speed larger than that of a thermal neutron ensures that the difference in counting rates between the two prisms (Prism 2–Prism 4) provides a selective measure of the flux of thermal neutrons coming from Mars [*Feldman and Drake*, 1986].

[15] The procedure used to reduce raw counting rates returned by MONS to thermal and epithermal neutron currents is given by *Prettyman et al.* [2004] and *Maurice et al.* [2007]. These currents are then translated into the WEH abundance of a semi-infinite layer of hydrogen-containing soil having an assumed range of compositions. The top layer has the same composition as that of the bottom layer, but containing a WEH abundance of 1 wt. % [see, e.g., *Diez et al.*, 2008, and references therein]. The burial depth of the bottom layer is also determined from this model. Because this technique is sensitive to burial mass, units are given in g/cm^2, which can be translated to depth by dividing by the assumed density of the soil (1.5 g/cm^3).

2.5. Uncertainties
2.5.1. Thermal Model Assumptions

[16] The model assumes a simple two layer system that consists of a variable thickness of dry soil on top of a semi-infinite layer of permafrost. Thermophysical parameters of the layers are listed in Table 1 and are similar to those described by *Mellon et al.* [2004]. It is clear that natural systems can be more complicated than this simple model, but the nature of the seasonal temperature data prevents recovery of useful information about more complicated systems.

[17] The dust opacity (at visible wavelengths) was held constant at 0.30 (scaled to 6 mbar) to keep the data processing and fitting routines relatively simple. The TES data used for this study was from relatively clear and constant periods with visible dust opacities typically between 0.15 and 0.4 [*Smith*, 2004].

[18] To assess the potential bias that may be introduced into the derived permafrost depths and surface cover thermal inertias, we fit a typical set of surface temperature measurements as described above, except with visible wavelength dust opacity values of 0.15 and 0.45 (Figure 1). These opacity values resulted in surface cover inertias of 261 and 285 and permafrost depths of 7.1 and 7.6 cm for opacity values of 0.15 and 0.45 respectively. The factor of 3 difference in atmospheric dust opacities has a <10% effect on permafrost depth and surface cover thermal inertia determinations.

[19] The magnitude of the effects of factors that affect solar energy input to a surface are highly dependent on local time and season. This includes atmospheric dust parameters such as total opacity and scattering properties and surface albedo properties. While the physics involved in accounting for these properties are well understood, the actual values to use for Martian properties are not. This can result in very large uncertainties in derived thermophysical parameters regardless of the sophistication of the thermal model used for their derivation.

[20] To illustrate this point, we modeled surface temperatures for a surface similar to that shown in Figure 1 except using temperatures from a local time of 1400 (Figure 2). The visible wavelength opacity values were varied in this case from 0.15 to 0.30. This variation is typical of 9 μm infrared opacity values of $\sim$0.08 to 0.15 [e.g., *Wolff and Clancy*, 2003]. Both *Wolff and Clancy* [2003] and *Bandfield and Smith* [2003] found TES 9μm dust opacity values to be significantly higher than the standard official TES opacities
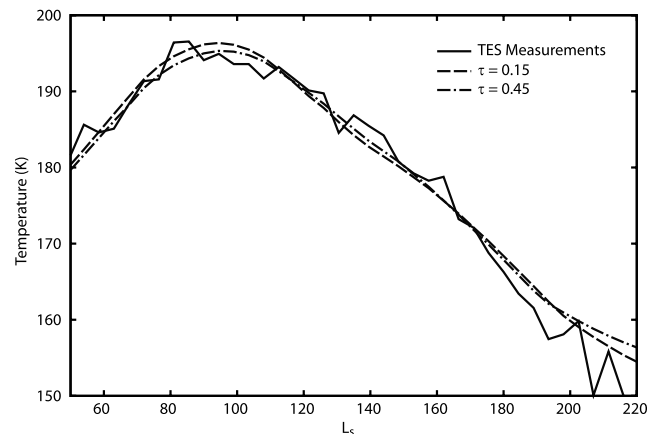

Figure 1. Changing atmospheric dust opacity (τ) has small effects on the modeled surface cover thermal inertia and permafrost depth. TES data (solid) from 67°N, 106°E is modeled with the algorithm described in the text using a surface cover thermal inertia of 261 with a permafrost depth of 7.1 cm assuming a visible wavelength opacity of 0.15 (dashed). Assuming an opacity of 0.45 results in a modeled surface cover thermal inertia of 285 and permafrost depth of 7.6 cm (dash-dot).
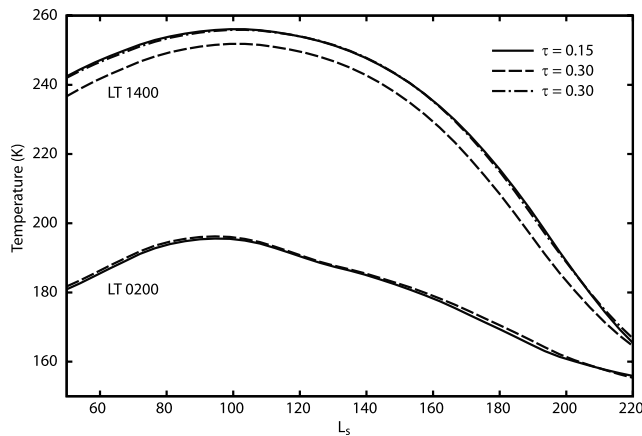
Figure 2. Effect of atmospheric dust opacity (τ) on surface temperature is much greater at a local time (LT) of 1400 than 0200. Two modeled temperature curves are for visible wavelength opacities of 0.15 (solid) and 0.30 (dashed) at 67°N, 106°E with a surface cover thermal inertia of 280 and permafrost at 7.6 cm. A third example (dash-dot) displays modeled temperatures for a surface cover thermal inertia of 150 and permafrost depth of 2.3 cm was necessary to fit the 1400 LT and opacity of 0.15 temperatures using an opacity of 0.30. Similar trends are apparent for other factors that affect solar input, such as albedo and dust scattering properties.

[*Smith et al.*, 2000], which were derived using a simple and computationally efficient method. As a result, these values and this range of uncertainty are typical for the TES data set.

[21] Unlike the 0200 local time example described above, the effects of changing atmospheric opacity on the derived thermophysical parameters from afternoon measurements are large. The change in dust opacity had a <1 K and 4−8 K effect on the 0200 and 1400 local time temperatures respectively. In order to adequately model temperatures from a surface cover thermal inertia of 280 and permafrost at a depth of 7.6 cm using a visible opacity of 0.30 instead of 0.15, the thermal inertia was lowered to 150 and the permafrost depth was changed to 2.3 cm (Figure 2). This uncertainty results in a significant mischaracterization of the surface.

[22] This high level of uncertainty was the reason we avoided the afternoon measurements. It is necessary to resolve these uncertainties (e.g., via thermophysically derived albedos [e.g., *Paige et al.*, 1994]) before measurements acquired at low angles of solar incidence can be used for derivation of surface thermophysical properties.

2.5.2. Surface Temperature Uncertainties

[23] Even with only a few observations in a bin, the systematic uncertainties in surface temperature due to surface emissivity, calibration, and atmospheric effects dominate over any random uncertainties due to instrument noise. In addition, heterogeneities within each latitude/longitude bin may be represented in a nonrandom manner within each L_s bin.

2.5.2.1. Random Variations

[24] The TES surface temperatures appear to have a random noise component within each L_s bin. This may be due to a number of contributing factors, including spatial heterogeneities, interannual variations in surface and atmospheric conditions, random calibration effects, and possible short term variations in atmospheric conditions (i.e., weather). Because seasonal surface temperatures on average change slowly and smoothly, it is possible to gain a quantitative assessment of these random variations by differencing the TES seasonal temperature curve from a smoothed curve. Using the same example discussed above and shown in Figure 1, the difference between the actual and smoothed temperature curves has a standard deviation of 1.65 K. This is representative of the TES data for the surfaces included in this study. This noise is a good indicator of the limitation of model fits and indicates that where modeled/measured RMS errors are significantly greater than 1.65 K, the model is increasingly inaccurate.

2.5.2.2. Surface Emissivity Effects

[25] Surface emissivity effects can be a source of systematic error in the retrieval of surface thermophysical properties because of the effects on the radiative balance in the model and its effects on the derivation of surface temperature from the data. TES surface temperatures for surfaces colder than 220 K are derived from the brightness temperature at ∼20−25 μm assuming a surface emissivity of 0.95. This is appropriate for relatively coarse particulate low albedo surfaces, but fine particulate, high albedo surfaces have higher emissivities [e.g., *Bandfield and Smith*, 2003].

[26] The effects of assuming an emissivity of 0.95 rather than 0.98 is an overestimate of surface temperature by 1− 2 K. Once again using the same example TES data as shown in Figure 1, the effect of this difference in surface emissivity assumed both in the thermal model and in derivation of surface temperature can be quantified. Assuming an emissivity of 0.98 versus 0.95 causes the derived surface cover thermal inertia to decrease from 272 to 237 and the derived permafrost depth to change from 7.3 to 6.4 cm. This is a potential 12−13% error that may be present depending on the nature of the surface.

2.5.2.3. Probable Breakdown of Thermophysical Retrievals at Lower Latitudes

[27] The derivation and modeling of surface temperatures requires an accurate understanding of atmospheric conditions. The thermal model used here as well as other models do not incorporate dynamic aspects of the Martian atmosphere and, as a result, do not account for heat transport via Hadley circulation from low latitudes to high latitudes and from the southern hemisphere to the northern hemisphere [e.g., *Leovy*, 2001]. This effect is most pronounced at northern midlatitudes during the fall season as relatively intense heating of the southern hemisphere near Mars perihelion sets up a vigorous transport of heat to the northern hemisphere south of the polar vortex [*Conrath et al.*, 2000].

[28] This has two compounding effects: (1) Surface temperature retrieval algorithms will overestimate surface temperatures by as much as 10 K from spectral measurements (and by considerably more from bolometer measurements). This effect is shown in Figure 3. (2) A relatively warm atmosphere will have a warming effect on nighttime surface temperatures that will not be accounted for by the thermal model. This effect is most pronounced at relatively low latitudes with low thermal inertia surface cover where the surface-atmosphere temperature contrast is greatest
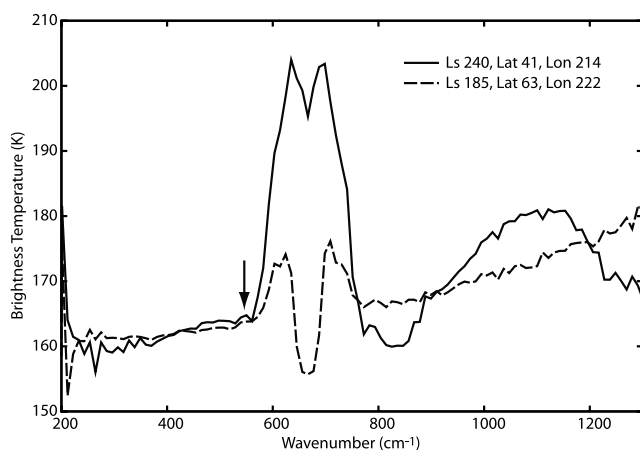
Figure 3. Atmospheric aerosols and CO_2 can have significant effects on retrieved surface temperatures. The solid line displays a TES spectrum from middle northern latitudes where the atmosphere is very warm due to Hadley transport of heat from the south. Radiance from both CO_2 (centered at 667 cm^{-1}) and dust are in positive relief causing the retrieved surface temperature to be overestimated at 165 K, ~5−10 K warmer than the actual surface temperature. The dashed line displays TES data from farther north where the atmosphere is close to the surface temperature and has little effect on the retrieved surface temperature of 164 K. The arrow denotes the approximate wavelength used for the surface temperature determination.

(~30−50° N, L_s ~180−300). Under these conditions, no combination of surface cover thermal inertias and permafrost depths could adequately model the measured surface temperatures (Figure 4). The apparent warming of the surface through the fall season has the effect of mimicking a shallow permafrost layer and will result in artificially shallow permafrost depth retrievals. As a result, we have restricted our data to latitudes greater than 50°, where these effects are not apparent (Figure 1). It is important to note that these effects also may influence other Martian thermophysical studies.

2.5.2.4. Sensitivity to Surface Cover Thermal Inertia and Permafrost Depth

[29] Surface cover thermal inertia and permafrost depth have different effects on seasonal surface temperatures that allows for a relatively robust separation of their effects [*Bandfield*, 2007]. For the summer/early fall ~0200 local time measurements used here, surface cover thermal inertia generally controls overall seasonal temperatures with higher temperatures indicative of higher thermal inertia values. The depth of the permafrost affects the overall rate of cooling through the late summer and early fall seasons (Figure 5). In a generalized sense, the surface cover thermal inertia controls the offset and the permafrost depth controls the slope of the seasonal temperature curve.

[30] The sensitivity to the depth of the permafrost layer and surface cover thermal inertia is dependent on a number of parameters. A strong seasonal cycle provides significant leverage for permafrost depth determination, but a short frost free season at high latitudes reduces the time and number of measurements available. High latitudes also

reduce the sensitivity to the surface cover thermal inertia because of a relatively weak diurnal solar cycle (Figure 6). The values of permafrost depth and surface cover thermal inertia also influence their own sensitivities. For example, at greater depths a change in the depth of the permafrost will have a diminished effect relative to the same change at shallower depths.

[31] To quantify the sensitivity to surface cover thermal inertia and permafrost depth, partial derivatives of RMS fitting error with respect to change in depth and surface cover thermal inertia were calculated for each latitude/longitude bin. This accounts for the unique conditions within each bin.

2.5.2.5. Neutron Spectrometer Uncertainties

[32] Resultant maps of bottom layer WEH concentration and burial depth from the MONS data have four major sources of uncertainty. The first reflects a combination of statistics, drifts in instrumental operating parameters, and variations in the intensity of cosmic rays. Together, these amount to ±5% for both the thermal and epithermal neutron currents [*Diez et al.*, 2008]. The second reflects our need to choose a depth-independent elemental composition of the near surface of Mars and the WEH content of the top-most layer. We have estimated these uncertainties by comparing values of bottom layer WEH concentration and burial depth returned by two-layer models having different compositions and WEH contents of the top-most layer. Estimates of the uncertainty caused by our lack of knowledge of the elemental composition was made using Monte-Carlo simulations of Prism 1 and Prisms 2−4 counting rates [*Prettyman et al.*, 2004]. These estimates used compositions that reflected the full width at half maximum value of a histogram of macroscopic neutron absorption cross sections of the regolith samples measured using the APXS experiment aboard the MER rovers [*Diez et al.*, 2008]. The uncertainty caused by our lack of knowledge of top layer
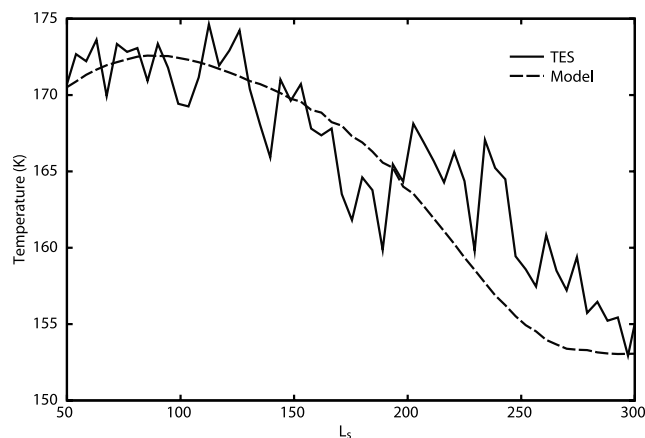

Figure 4. TES surface temperatures from 41°N, 214°E (solid) are poorly modeled (dashed) for the midlatitude example location shown in Figure 3. Surface temperatures slow their seasonal decline past Ls ~200 due to atmospheric effects described in the text. The extra warming past this point prevents the thermal model from adequately fitting the seasonal temperature curve. The modeled temperatures have a surface cover thermal inertia of 84 with a permafrost depth of 1.3 cm and an RMS error of 2.8 K.
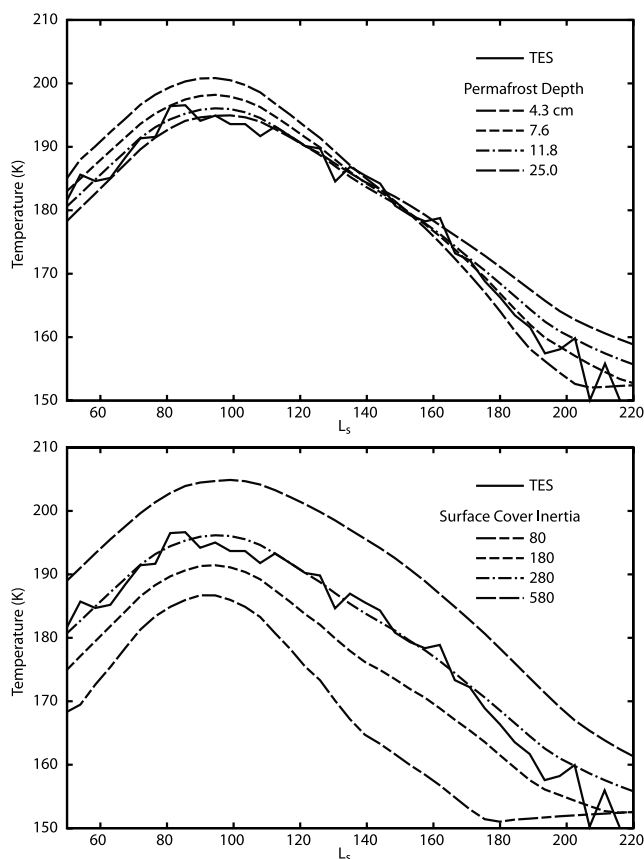
Figure 5. Changes in permafrost depth affect the rate of seasonal cooling (top) and changes in surface cover thermal inertia affect the overall seasonal surface temperatures (bottom). The example shown is for a local time of 0200 at 67°N, 106°E as in previous figures.

WEH abundance was estimated by comparing bottom layer WEH abundance and burial depth values returned under the assumption of top layer WEH abundances of 1% and 5%. Although estimates for top layer WEH abundance derived from near-infrared spectral absorption measurements from Mars Express Observatoire pour la Mineralogie, l'Eau, les Glaces et l'Activité (OMEGA) data for latitudes poleward of 60°N can be greater than 5% [*Milliken et al.*, 2007], we capped our procedure at 5% because the cloud of fast and epithermal neutron currents measured using MONS at latitudes between 60° and 75° fall far outside the grid of physically realistic values [*Feldman et al.*, 2007]. The discrepancy between the results inferred from near infrared measurements and MONS data is likely due to the shallow depth of sensitivity of the near infrared measurements, which are not likely to be representative of the bulk regolith beyond the upper 10s to 100s of μm.

[33] Our estimates of bottom layer WEH abundance and depth uncertainties due to uncertainties in composition and top layer WEH abundance are shown in Figure 7. Starting first with our assumption of top layer WEH abundance of 1%, our derived values for both bottom layer WEH abundance and depth will be systematically low (Figures 7a and 7b). Both uncertainties are smaller at higher latitudes where bottom layer WEH abundance is highest and the burial

depth is smallest. Uncertainties in bottom layer WEH abundance and burial depth in the latitude range between 65° and 75° due to uncertainties in soil composition are shown in Figures 7c and 7d, respectively. The data shown in Figure 7 indicate that these uncertainties amount to roughly ±0.03% mass fraction derived from the assumption of the most probable composition, and ±10% for the depth.

[34] An estimate for the uncertainties in bottom layer WEH abundance and depth that stem from the spatial heterogeneity of the Martian surface within the MONS field of view (about 600 km diameter) cannot be derived from MONS data alone. The only way to fix a level for this uncertainty is to compare the bottom layer WEH abundance and burial depth determined using MONS data with those returned by analyses of other experiments that have better spatial resolution and that require distinct models of near-surface conditions. Such a comparison is one of the goals of our present study.

3. Results

[35] Surface cover thermal inertia, permafrost/water-ice depth, and error maps are displayed in Figures 8 and 9. There are clear correlations between the different data sets and derived parameters. For example, between ~50°–
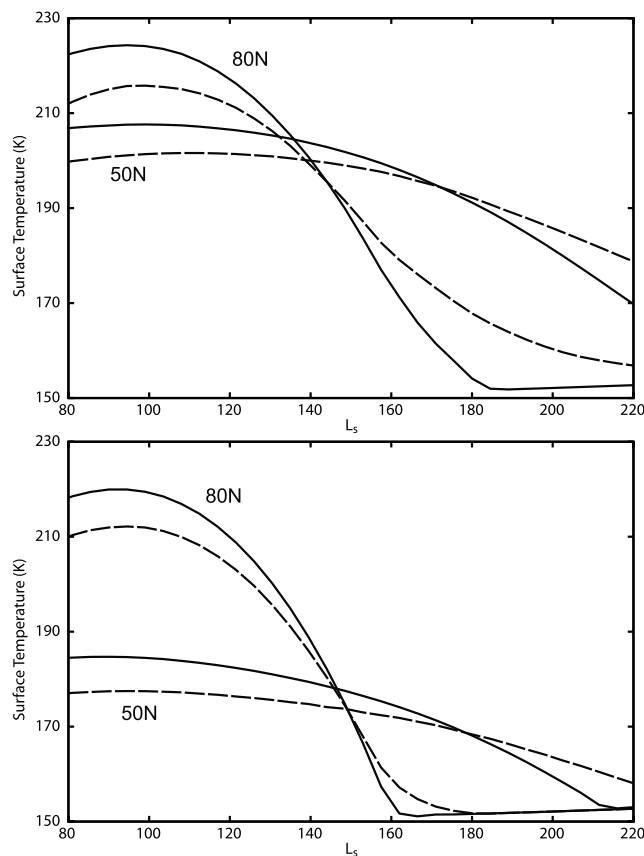

Figure 6. Latitude, surface cover thermal inertia, and permafrost depth affect their impact on surface temperature. Modeled temperatures are for latitudes 50°N (shallow sloped lines) and 80°N (steep sloped lines), surface cover thermal inertias of 100 (top plot) and 500 (bottom plot), and permafrost depths of 1.15 (dashed lines) and 20.3 (solid lines) diurnal skin depths.
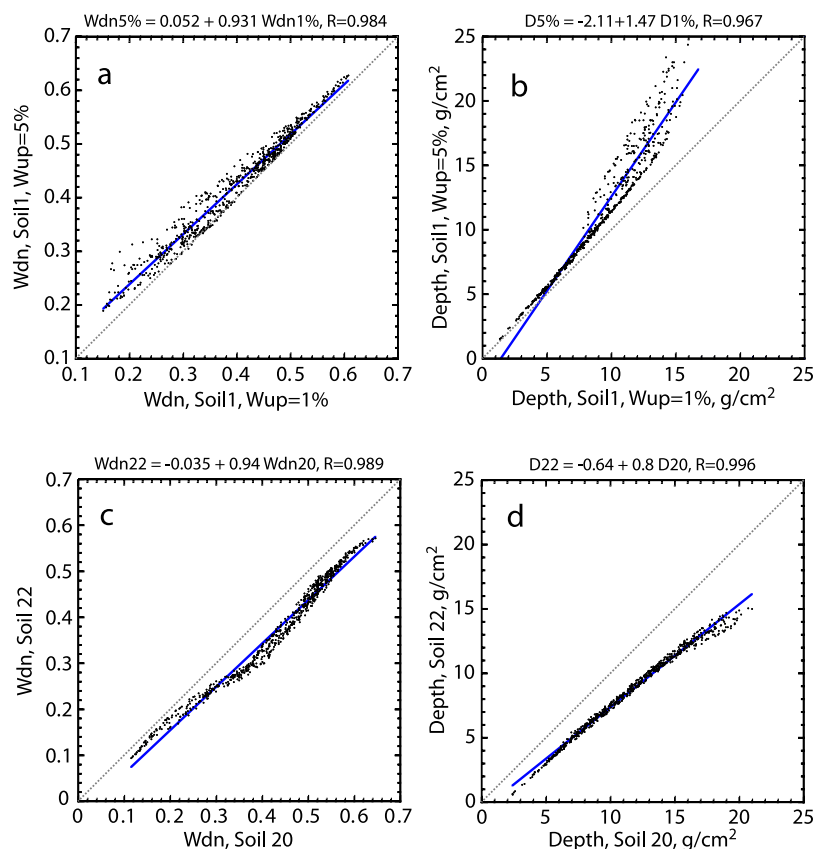
Figure 7. Effects of uncertainties in soil composition and water equivalent hydrogen (WEH) abundance on bottom layer WEH abundance and burial depth are shown in Figures 7a–7d. All data are taken from $60°-75°$N/S latitude with individual bins shown as points. The associated linear regression (solid line) is listed at the top of each plot. Soils 1, 20, and 22 are various assumed regolith compositions that are described in detail by *Diez et al.* [2008]. Wup and Wdn are the top and bottom layer WEH abundances respectively and Depth is the burial depth of the bottom layer.

$65°$N, relatively low albedo surfaces are associated with relatively high surface cover thermal inertias, neutron derived water ice depths, and surface temperature derived permafrost depths. Similar spatial correlations are also apparent in the southern hemisphere maps, although the nature of the surface cover thermal inertia and the permafrost/water-ice distributions are significantly different from the northern hemisphere maps.

[36] Although there is a strong correlation between albedo, surface cover thermal inertia, and permafrost depth, there are regions where these patterns break down. A noticeable example is the region of high surface cover thermal inertia between $72°-76°$N and $30°-150°$E. In this region the albedo remains relatively high and there is no corresponding increase (in skin depths) in the permafrost depth.

[37] Several differences are also immediately apparent between the maps. While there is a qualitative agreement in the spatial pattern of surface temperature derived permafrost depths and neutron derived water ice depths, the neutron derived data does not display as great depths as those derived from the surface temperature data. There appears to be an exponential relationship between the two data sets (Figure 10). At shallow depths (<15 g/cm^2) there appears to be a rough correlation between the two data sets.

[38] Average RMS errors are 1.93 K and 2.30 K in the north and south respectively. This excludes regions of permanent water or CO_2 ice, which will not be well fit by the model. The southern hemisphere has no prominent regions of elevated error, but contains apparently random regions of higher RMS errors. These regions have no apparent correlation with the derived permafrost depths or surface cover thermal inertia. A possible cause of this noise is the spatially random inclusion of data from periods of elevated dust opacity during the southern summer. The northern hemisphere has slightly improved fits at lower latitudes with the exception of near $230°-300°$E. There is some association of lower RMS errors with greater permafrost depth and surface cover thermal inertia.

4. Discussion

4.1. Spatial Distribution of Permafrost Depths

[39] A qualitative comparison of Neutron Spectrometer hydrogen and TES permafrost depths displays remarkable agreement considering the fundamental difference in the measurements (Figures 8 and 9). Many of the differences in detail can be attributed to the measurement resolutions. These differences largely disappear by filtering the TES
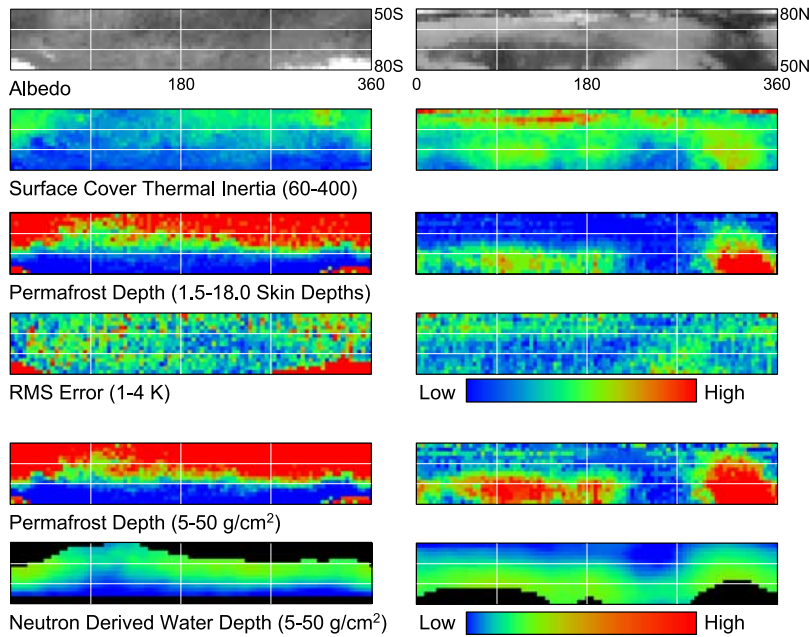
Figure 8. Albedo, surface cover thermal inertia, permafrost depth, neutron derived water depth, and RMS error maps are shown for $50°-80°$N/S at all longitudes. The bottom set of four depth maps (Permafrost Depth and Neutron Derived Water Depth) are in burial depth assuming a 1.5 g/cm^3 surface cover bulk density and use the bottom logarithmic color scale.

results with a boxcar filter 10° latitude and 20° of longitude wide to roughly simulate the Neutron Spectrometer spatial resolution (Figure 9).

[40] In the northern hemisphere, water ice and permafrost depths are greater within lower latitude, higher surface cover thermal inertia, and low albedo regions. This shows that the water ice depth is generally following its predicted stability as all three of these properties generally increase the depth of water ice stability. At higher latitudes, all surfaces are characterized by shallow water ice depths. This includes the low albedo polar sand dune surfaces, consistent with the results of *Feldman et al.* [2008].

[41] In the southern hemisphere, water ice/permafrost depths are shallow at latitudes $>\sim 65°$S. A relatively steep increase in depths appears between $60°-65°$S that, as in the north, coincides with an increase in surface cover thermal inertia and a decrease in latitude and albedo. This is

relatively constant with longitude except between $\sim 50°-140°$E near Malea Planum, Promethei Terra, and the southern rim of Hellas Basin. In these regions, the surface cover thermal inertia remains low and the albedo is relatively high, which allows for water ice to remain stable at relatively shallow depths at lower latitudes.

[42] The primary difference between the two data sets is present near $53°-63°$N and $210°-270°$E. The neutron derived depths show a region of greater hydrogen depths where the temperature derived permafrost depths remain shallow throughout this region. The TES data display elevated RMS errors in this region that may provide a possible explanation for this discrepancy. It is a low surface cover thermal inertia region at mid latitudes. Because of its relatively low latitude and low nighttime temperatures, this region may be somewhat affected by the lack of modeling the atmospheric dynamics as discussed above in section 2.5.
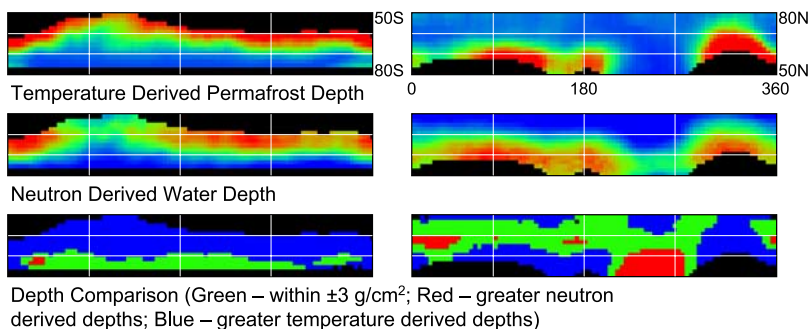

Figure 9. Temperature derived permafrost (top) and neutron derived water depth maps (middle) similar to those shown in Figure 8 as well as depth comparison maps (bottom). The permafrost depths have been spatially filtered to approximately the same resolution as the neutron measurements and have had the same mask applied. The depth maps have been individually stretched to show their spatial correlation.
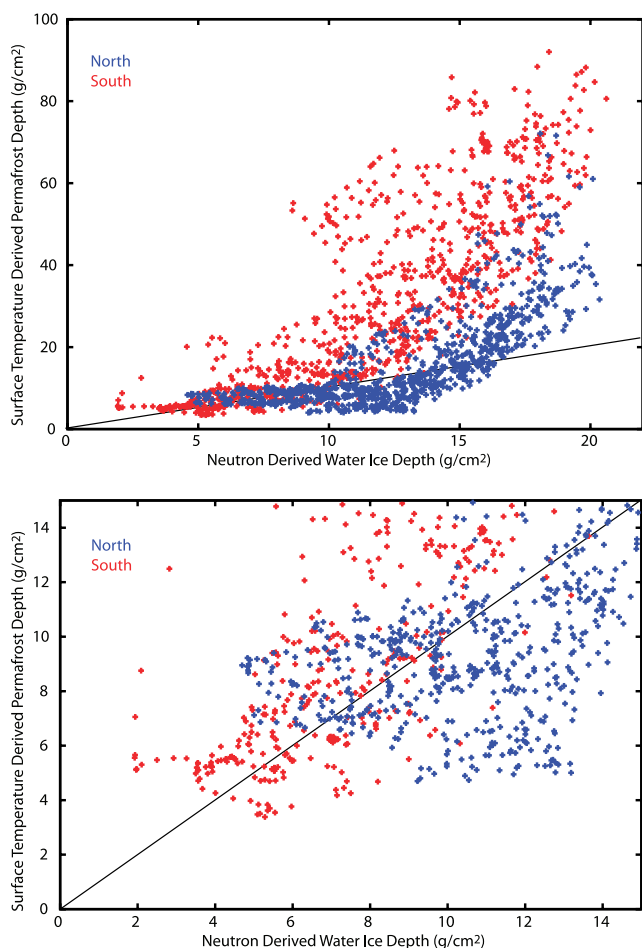
Figure 10. Temperature derived permafrost depths have a nonlinear relationship to the neutron derived water depths that is apparent at greater burial depths (top). In addition, northern regions (blue) have a different correlation than southern regions (red) at greater burial depths. The bottom plot contains the same data as the top, but with a limited range to show detail at shallow burial depths. The permafrost depths assume a 1.5 g/cm^3 surface cover density.

4.2. Quantitative Comparison of Derived Water Ice Depths

[43] Despite the similar spatial patterns present in the neutron and temperature derived water ice depths, there are systematic quantitative differences (Figures 9 and 10). Part of this discrepancy may be explained by differences in the depths of sensitivity of the two techniques. The temperature measurements are limited to depths greater than ∼1 diurnal skin depth and, as discussed below, permafrost and surface cover thermal inertia may not be well distinguished at <2−3 diurnal skin depths (∼5−8 cm for a surface thermal inertia of 200). To determine shallower permafrost depths, more complete diurnal temperature coverage is required. Conversely, effects of uncertainties in soil cover composition and water content on the water ice depths derived from neutron measurements become significant at greater than ∼20 g/cm^2 (∼13 cm). As a result, the two techniques do not have a great deal of overlap in their depths of greatest sensitivity.

[44] Despite the fact that these uncertainties may account for the discrepancy between the derived burial depths, there may also be a physical explanation as well. At greater burial depths, the neutron measurements may be more sensitive to layered hydrated minerals closer to the surface than more deeply buried deeper water ice. In essence, the simple two layered model is skewed by the hydrated layer that will have a more significant effect on the measured neutron signal than more deeply buried water ice. It is worth noting that low latitude hydrated mineralogies in regions such as Arabia Terra inferred from MONS data [e.g., *Feldman et al.*, 2004] may reasonably be assumed to be present at high latitudes. Indeed, similar to ice, many hydrated compositions will be more stable in higher latitude regions.

[45] If both the neutron and temperature measurements are indeed accurately detecting buried water ice, an additional explanation for the discrepancy in derived depths may lie in the simplistic assumptions of a two layered dry regolith/icy permafrost model. *Feldman et al.* [2007] showed that the water ice concentration was strongly anti-correlated with burial depth. At burial depths of 20 g/cm^2, the derived water equivalent hydrogen concentration is ∼10 wt. %. Although these data may be indicative of reduced porosity at greater burial depths, it also may be interpreted as incomplete filling of pore space by water ice. This would result in a buried permafrost layer with a significantly lower thermal inertia than assumed for the two layer model used for the derivation of permafrost depths from the TES data. To compensate for this incorrect assumption, the fitting routine would derive an artificially high permafrost depth. This is because the lower thermal inertia layer would have less of an effect on the surface temperature than a higher thermal inertia layer at a similar depth. Preliminary work by *Titus and Prettyman* [2007] has indicated that variations in permafrost layer thermal inertia may indeed be present.

[46] The general agreement of the neutron and temperature derived water ice depths adds robustness to the accuracy of both data sets and techniques. However, where disagreements occur between the two sets of results may also lend insight into their inherent flaws as well as provide clues that the subsurface structure may be more complicated than can be described using the simple two layered model described here.

4.3. Surface Cover Thermal Inertia
4.3.1. Comparison With Previous Results

[47] Obtaining accurate surface cover thermal inertias at high latitudes is essential for prediction of theoretical water ice stabilities. This is, however, a particularly difficult determination because of a rather weak diurnal energy cycle and the influence of ice itself on the apparent thermal inertia at these latitudes.

[48] *Paige and Keegan* [1994] and *Paige et al.* [1994] used seasonal Viking Infrared Thermal Mapper (IRTM) temperature data to derive the apparent thermal inertia of Martian polar regions. Similar work was done by *Vasavada et al.* [2000] to characterize the Mars Polar Lander and Deep Space 1 Mars Microprobe landing sites and *Putzig et al.* [2005] derived thermal inertias at all latitudes using single nighttime temperature measurements. Despite some quantitative differences due to the models and type of data used,
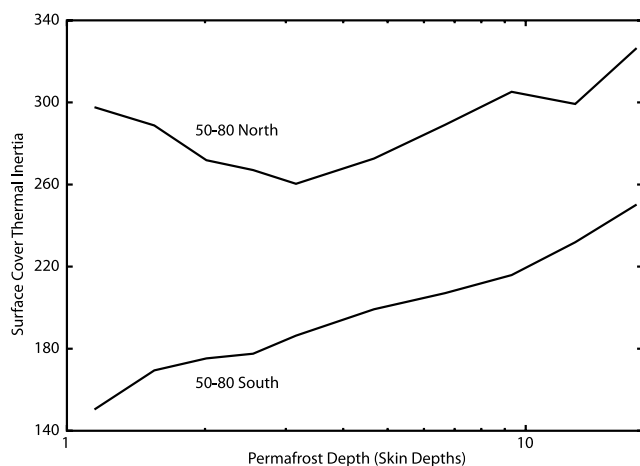
Figure 11. Average surface cover thermal inertia is generally positively correlated with permafrost depth and is offset between the northern and southern hemispheres. An exception to this correlation is at <2–3 skin depths in the Northern Hemisphere where the permafrost is likely shallow enough to be influencing diurnal temperature variations as discussed in section 4.3.

these studies show that thermal inertia in the northern hemisphere is generally higher than in the southern high latitudes.

[49] We find a similar pattern of surface cover thermal inertia here. The southern hemisphere has average surface cover thermal inertias of 159, 208, and 251 at 70°–80°, 60°–70°, and 50°–60°S respectively. This is in-between the relatively high values derived by *Paige and Keegan* [1994] and low values of *Vasavada et al.* [2000]. *Putzig et al.* [2005] have lower thermal inertia values between ~70°–80°S and higher thermal inertia values at ~50°–60°S. It is interesting to note that the southern rim of Hellas basin has high values of thermal inertia up to ~500 by *Putzig et al.* [2005], but is a region of low surface cover thermal inertia (~200) and relatively shallow permafrost here. As discussed below, this will have a significant effect on water ice stability depths predicted by vapor diffusion models.

[50] Where surface cover thermal inertia generally decreases poleward in the south, the pattern is more complex in the north. Elevated thermal inertias values of ~300–400 are typical of low albedo regions such as Acidalia near 50°–65°N. This is about 50–150 units lower than those of *Paige et al.* [1994] and *Putzig et al.* [2005].

[51] One of the reasons that the term "apparent thermal inertia" is used for polar studies of surface thermophysical properties is that it is impossible to characterize a layered surface with a single value. Thermal inertia derived assuming a vertically homogeneous surface will not be constant based on season [e.g., *Putzig and Mellon*, 2008]. The work presented here is an improvement on previous studies because it explicitly accounts for vertical heterogeneity (albeit in a simplistic manner) and the surface cover thermal inertia values are likely more representative of the top layer of regolith.

4.3.2. Influence of Top Layer Inertia on Ice Depth

[52] Although a general pattern of increased permafrost depth with decreasing latitude is present globally, the surface cover thermal inertia is also highly correlated with permafrost depth (Figure 11). A surface with high thermal inertia conducts more energy into the subsurface and to a greater depth than a low thermal inertia surface cover. The correlation is offset between the north and the south because the greater energy input to the southern hemisphere during the summer increases the seasonal maximum temperature at the depth of the ice table (Figure 12).

[53] An exception to this correlation is at shallow depths (<2–3 skin depths) in the northern hemisphere. These shallow depths appear between 70°–80°N and are concentrated near regions of permanent water ice exposures detached from the main polar cap from ~90°–270°E. The most likely explanation for these high surface cover thermal inertia values is that the permafrost is shallow enough to influence the derived surface cover thermal inertia. These exposures are probably extensions of the exposed ice deposits covered by a lag deposit of residual dust. There is no similar pattern apparent in the southern hemisphere data despite significant exposures of water ice [*Titus et al.*, 2003; *Bibring et al.*, 2004].

[54] The shallow water ice exposures in the northern hemisphere show that water ice may be out of equilibrium and actively receding. With the permafrost at or less than 1.15 skin depths (the shallowest allowed by the fitting algorithm), these ice exposures are not well insulated from large diurnal temperature variations and the permafrost layer can exceed 215 K in the model (which does not account for the energy involved in sublimation of water ice). It may be possible that model assumptions could have an influence on the depth determination, however. A thermal conductivity of the permafrost layer that is significantly higher than assumed or surface cover thermal inertia that is significantly lower than allowed by the model will result in lower permafrost temperatures. For example, if the surface cover thermal inertia is extremely low (20 J m^{-2} K^{-1} s$^{-0.5}$), water ice may be stable at depths of <0.001 m and provide a reasonable match to the measured seasonal temperatures. It is impossible without more complete diurnal temperature measurements to determine the true surface cover thermal inertia and burial depths at these locations. These thermal inertia values are not likely to be representative of the surface cover and should not be used for modeling theoretical ice depths based on vapor diffusion and other models. The lack of a similar situation in the southern hemisphere may be indicating that the southern hemisphere is closer to equilibrium permafrost conditions than the northern hemisphere.

4.4. Comparison With Vapor Diffusion Models

[55] Both *Mellon et al.* [2004] and *Schorghofer and Aharonson* [2005] developed models to predict the stability depth of water ice in the current Martian climate. These models are based on free exchange of water vapor between the subsurface and atmosphere in addition to updated thermal models, thermal inertia data, and water vapor measurements. The model results compared favorably with the locations of significant concentrations of hydrogen detected by the Neutron Spectrometer measurements. As this work was performed before the more recent layered results, no comparison of predicted versus derived burial depths was done. A more quantitative comparison was performed by *Diez et al.* [2008], which found significant
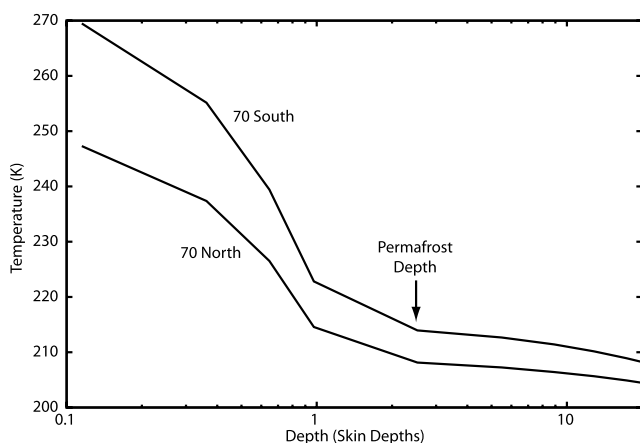
Figure 12. Maximum annual temperature is greater in the Southern than the Northern Hemisphere, which accounts for the offset in permafrost depths shown in Figure 11. In this example, surface cover thermal inertia is 200, frost free albedo is 0.20, and permafrost is located at 1.15 surface cover diurnal skin depths. The mean annual temperature is greater in the Northern Hemisphere and the temperature curves cross beyond the range of the graph at ~80 skin depths (~2.3 m) as the seasonal temperature variations are considerably reduced at greater depths.

discrepancies between the burial depths of both models and the neutron measurements.

[56] The results discussed here may provide some insight into these differences. First, significant uncertainties exist in the thermophysical properties of the surface material at high latitudes. This can have a dominant effect on water ice stability depths predicted by *Mellon et al.* [2004] and *Schorghofer and Aharonson* [2005]. Both of these studies used TES derived thermal inertia values similar to those of *Putzig et al.* [2005] up to 80° latitude.

[57] Two areas of poor agreement between the vapor diffusion models and the neutron and temperature derived water ice depths are the southern rim of Hellas Basin and high northern and southern latitudes between ~70°–80°. These regions coincide with disagreements in the thermal inertia values derived by *Putzig et al.* [2005] and the surface cover thermal inertias presented here. Where the thermal inertia values of *Putzig et al.* [2005] are higher (high northern latitudes and southern rim of Hellas Basin), model predicted depths are greater than either the neutron or temperature derived depths. Where they are lower (high southern latitudes), model predicted depths are less than those presented here. Thermal inertia data derived without incorporating the thermophysical effects of buried water ice will cause inaccuracies when used for the prediction of water ice stability depths.

[58] The vapor diffusion models assume equilibrium conditions, which may be an additional potential source of disagreement with the water ice depths derived from the neutron and temperature measurements. As described above, large regions in the northern high latitudes are shallow enough that they may be actively receding. These regions coincide with surface cover thermal inertias that are likely too high and it is not possible to decouple the two

possible causes for the discrepancy between the depths derived from measurements and the model predictions.

4.5. Comparison of Regional Results With Local Distributions From THEMIS

[59] It is clear that there are regional variations in permafrost depth and surface cover thermal inertia at the scale of the TES and Neutron Spectrometer measurements. While this provides a general picture of the nature of the surface and subsurface within a region, local heterogeneities can display more variation than what is apparent regionally [*Sizemore and Mellon*, 2006; *Aharonson and Schorghofer*, 2006; *Bandfield*, 2007]. Local slopes, surface cover thermal inertia, and albedo can all have significant effects on the depth of the permafrost. For example, a poleward facing slope or a dusty patch will reduce the amount of heat conducted into the subsurface and will shallow the depth of permafrost stability. Rockier, low albedo, and equator facing surfaces will have the opposite effect. Permafrost depths have been shown to have this variability at the sub-km scale [*Bandfield*, 2007].

[60] Figure 13 displays permafrost depths determined from THEMIS seasonal temperature data over the region of the 2007 Mars Scout Phoenix spacecraft landing site [*Arvidson et al.*, 2007]. The data were processed in a manner similar to that described by *Bandfield* [2007]. Average inertia and depth retrieved from the TES data for the region is 258 and 4.5 cm respectively. The THEMIS data has slightly higher values of 283 and 6.2 cm. There is good agreement between these data sets especially considering the relatively high uncertainties in absolute permafrost depth determinations from THEMIS data [*Bandfield*, 2007]. This comparison shows that the low resolution measurements retain an overall accuracy, but are also not able to resolve a large amount of detailed variability that is clearly present.

[61] Spatial variability in water ice/permafrost depths is present at all scales and the THEMIS data provides an important bridge between the 10s to 100s of km scales of the TES and Neutron Spectrometer measurements and the <1 m scales to be accessed by the 2007 Mars Scout Phoenix lander. THEMIS data will be important for placing the Phoenix observations in the regional and global context presented here.

4.6. Emplacement Mechanisms

[62] There has been a remarkable amount of recent progress in the characterization of the subsurface water that has been predicted to be present for decades. Despite this, there is still uncertainty about the nature of the emplacement of the water ice. Models based on diffusion of water vapor between the surface and the subsurface generally predict where the water is near the surface if not precisely the depth. However, it is difficult to explain the extremely large concentrations determined from the Gamma Ray Spectrometer suite of measurements by vapor diffusion into open pore space. There may be other processes that serve to concentrate the ice, such as ice lensing that may at least partially account for these large concentrations [*Feldman et al.*, 2007].

[63] An additional process that may account for the current distribution of water ice deposits and depths is
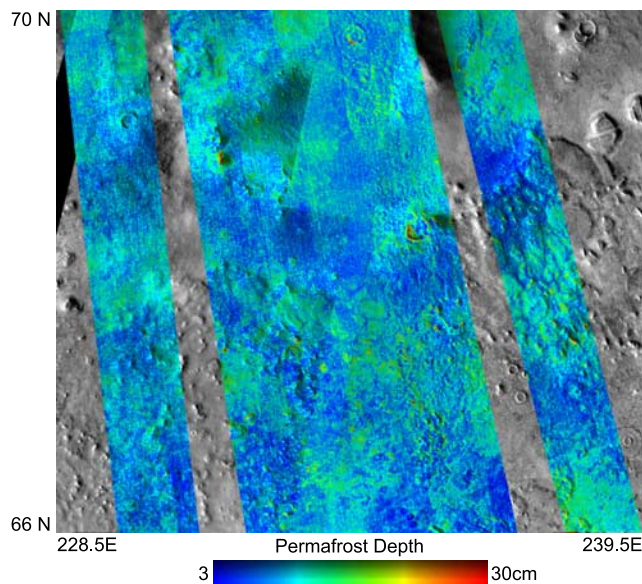
Figure 13. Permafrost depths derived from THEMIS seasonal temperature data are in reasonable agreement with the TES data from the same region. The area shown here includes the primary landing site for the Phoenix spacecraft. The region shown is approximately 250 km across.

sublimation of past surface deposits and formation of a surface cover lag. Presumably this lag would consist of air fall dust deposits that fell on their own or as condensation nuclei for the ice. In such a case, the surface cover thermal inertia would be expected to be quite low. This is indeed the case in the southern hemisphere, but there are locations in the northern hemisphere, such as the Vastitas Borealis formation and the polar sand seas that clearly have significant rock and sand deposits that are not consistent with a residual lag of dust.

[64] It is possible, and indeed likely, that the current distribution of water ice is attributable to both recession of residual surface ice deposits as well as emplacement via vapor diffusion [*Schorghofer*, 2007]. As with the polar layered deposits, the subsurface distribution of the water ice may be more complicated than an icy/not-icy model that the simple nature of the data sets restrict us to. Climate cycles can be variable in both magnitude and duration and these variations may leave their imprint on the subsurface water distributions, especially because it is possible that their response times to the climate cycles may not be instantaneous.

5. Conclusions

[65] This work has shown that high latitude seasonal surface temperatures on Mars can be well modeled by assuming a variable thermal inertia surface cover and depth of a buried permafrost layer. The depth to the permafrost layer is correlated with surface cover thermal inertia, albedo, and latitude in general agreement with predicted trends of water ice stability.

[66] Significant uncertainties are present when modeling surface temperatures with low angles of solar incidence.

Low thermal inertia midlatitude surfaces can also have significant uncertainties because atmospheric dynamics and heat transport are not incorporated in many thermal models.

[67] Comparison of permafrost depths with water ice rich layer depths derived from MONS data displays good qualitative agreement. There appears to be a divergence in the measured burial depths at greater depths. This disparity may be due to the presence of hydrated minerals at shallow depths or a lower than expected permafrost inertia corresponding with low water ice concentrations at greater depths.

[68] Surface cover thermal inertias are greater in the northern high latitudes than in the south, in agreement with previous studies that did not incorporate a two layer model. Quantitative differences between these results will have significant effects on the predicted Martian water ice stability, especially in regions such as the southern rim of Hellas Basin.

[69] Several regions in the northern hemisphere display high surface cover thermal inertia associated with shallow permafrost depths. This is likely due to water ice deposits that are shallow enough to influence diurnal surface temperatures. These regions are possibly actively receding, especially as they are near isolated regions of permanent exposed water ice.

[70] Significant lateral and vertical heterogeneity in water ice distributions are present. Variability in permafrost depths occur at scales much finer than those of TES or MONS. Despite this variability, the regional depth determinations are similar to an average of the finer scale observations derived from THEMIS data. The relationships between the TES and MONS derived permafrost and water ice depths, surface cover thermal inertias, and MONS derived water ice concentrations indicate that the Martian regolith is probably more complicated than can be described by simple two layered models and a single mode of emplacement.

References

Aharonson, O., and N. Schorghofer (2006), Subsurface ice on Mars with rough topography, *J. Geophys. Res.*, *111*, E11007, doi:10.1029/2005JE002636.

Armstrong, J. C., T. N. Titus, and H. H. Kieffer (2005), Evidence for subsurface water ice in Korolev crater, *Mars Icarus*, *174*, 360–372.

Arvidson, R. E., et al. (2007), Overview of Mars exploration program 2007 phoenix mission landing site selection, *Lunar Planet. Sci.*, *38*, 3204.

Bandfield, J. L. (2007), High-resolution subsurface water-ice distributions on Mars, *Nature*, *447*, 64–67.

Bandfield, J. L., and C. S. Edwards (2008), Derivation of Martian surface slope characteristics from directional thermal infrared radiometry, *Icarus*, *193*, 139–157, doi:10.1016/j.icarus.2007.08.028.

Bandfield, J. L., and M. D. Smith (2003), Multiple emission angle surface-atmosphere separations of thermal emission spectrometer data, *Icarus*, *161*, 47–65.

Bibring, J.-P., et al. (2004), Perennial water ice identified in the south polar cap of Mars, *Nature*, *428*, 627–630.

Boynton, W. V., et al. (2002), Distribution of hydrogen in the near surface of Mars: Evidence for subsurface ice deposits, *Science*, *297*, 81–85.

Boynton, W. V., et al. (2004), The Mars Odyssey gamma-ray spectrometer instrument suite, *Space. Sci. Rev.*, *110*, 37–83.

Christensen, P. R., et al. (2001), Mars Global Surveyor Thermal Emission Spectrometer experiment: Investigation description and surface science results, *J. Geophys. Res.*, *106*, 23,823–23,871.

Conrath, B. J., J. C. Pearl, M. D. Smith, W. C. Maguire, P. R. Christensen, S. Dason, and M. S. Kaelberer (2000), Mars Global Surveyor Thermal Emission Spectrometer (TES) observations: Atmospheric temperatures during aerobraking and science phasing, *J. Geophys. Res.*, *105*, 9509–9519.

Diez, B., W. C. Feldman, S. Maurice, O. Gasnault, T. H. Prettyman, M. T. Mellon, O. Aharonson, and N. Schorghofer (2008), H layering in the top meter of Mars, *Icarus*, in press.

Fanale, F. P., J. R. Salvail, A. P. Zent, and S. E. Postawko (1986), Global distribution and migration of subsurface ice on Mars, *Icarus*, *67*, 1–18.

Feldman, W. C., and D. M. Drake (1986), A Doppler filter technique to measure the hydrogen content of planetary surfaces, *Nucl. Instrum. Methods Phys. Res.*, *245*, 182–190.

Feldman, W. C., M. C. Bourke, R. C. Elphic, S. Maurice, J. Bandfield, T. H. Prettyman, B. Diez, and D. J. Lawrence (2008), Hydrogen content of sand dunes within Olympia Undae, *Icarus*, in press.

Feldman, W. C., M. T. Mellon, O. Gasnault, B. Diez, R. C. Elphic, J. J. Hagerty, D. J. Lawrence, S. Maurice, and T. H. Prettyman (2007), Vertical distribution of hydrogen at high northern latitudes on Mars: The Mars Odyssey Neutron Spectrometer, *Geophys. Res. Lett.*, *34*, L05201, doi:10.1029/2006GL028936.

Feldman, W. C., et al. (2002), Global distribution of neutrons from Mars: Results from Mars Odyssey, *Science*, *297*, 75–78.

Feldman, W. C., et al. (2004), Global distribution of near-surface hydrogen on Mars, *J. Geophys. Res.*, *109*, E09006, doi:10.1029/2003JE002160.

Fergason, R. L., P. R. Christensen, and H. H. Kienffer (2006), High-resolution thermal inertia derived from the Thermal Emission Imaging System (THEMIS): Thermal model and applications, *J. Geophys. Res.*, *111*, E12004, doi:10.1029/2006JE002735.

Jakosky, B. M., M. T. Mellon, H. H. Kieffer, P. R. Christensen, E. S. Varnes, and S. W. Lee (2000), The thermal inertia of Mars from the Mars Global Surveyor Thermal Emission Spectrometer, *J. Geophys. Res.*, *105*, 9643–9652.

Leighton, R. R., and B. C. Murray (1966), Behavior of carbon dioxide and other volatiles on Mars, *Science*, *153*, 136–144.

Leovy, C. (2001), Weather and climate on Mars, *Nature*, *412*, 245–249.

Maurice, S., W. Feldman, T. Prettyman, B. Diez, and O. Gasnault (2007), Reduction of Mars Odyssey neutron data, *Lunar Planet. Sci.*, *38*, 1338.

Mellon, M. T., and B. M. Jakosky (1995), The distribution and behavior of Martian ground ice during past and present epochs, *J. Geophys. Res.*, *100*, 11,781–11,799.

Mellon, M. T., B. M. Jakosky, H. H. Kieffer, and P. R. Christensen (2000), High-resolution thermal inertia mapping from the Mars Global Surveyor Thermal Emission Spectrometer, *Icarus*, *148*, 437–455.

Mellon, M. T., W. C. Feldman, and T. H. Prettyman (2004), The presence and stability of ground ice in the southern hemisphere of Mars, *Icarus*, *169*, 324–340.

Milliken, R. E., J. F. Mustard, F. Poulet, D. Jouglet, J.-P. Bibring, B. Gondet, and Y. Langevin (2007), Hydration state of the Martian surface as seen by Mars Express OMEGA: 2. H_2O content of the surface, *J. Geophys. Res.*, *112*, E08S07, doi:10.1029/2006JE002853.

Mitrofanov, I. G., M. L. Litvak, A. S. Kozyrev, A. B. Sanin, V. I. Tret'yakov, V. Y. Grin'kov, W. V. Boynton, C. Shinohara, D. Hamara, and R. S. Saunders (2004), Soil water content on Mars as estimated from neutron measurements by the HEND instrument onboard the 2001 Mars Odyssey Spacecraft, *Sol. Syst. Res.*, *38*, 253–257.

Paige, D. A. (1992), The thermal stability of near-surface ground ice on Mars, *Nature*, *356*, 43–45.

Paige, D. A., J. E. Bachman, and K. D. Keegan (1994), Thermal and albedo mapping of the polar regions of Mars using Viking thermal mapper observations: 1. North polar region, *J. Geophys. Res.*, *99*, 25,959–25,991.

Paige, D. A., and K. D. Keegan (1994), Thermal and albedo mapping of the polar regions of Mars using Viking thermal mapper observations: 2. South polar region, *J. Geophys. Res.*, *99*, 25,993–26,013.

Prettyman, T. H., et al. (2004), Composition and structure of the Martian surface at high southern latitudes from neutron spectroscopy, *J. Geophys. Res.*, *109*, E05001, doi:10.1029/2003JE002139.

Putzig, N. E., and M. T. Mellon (2008), Apparent thermal inertia and the surface heterogeneity of Mars, *Icarus*, *191*, 68–94, doi:10.1016/j.icarus.2007.05.013.

Putzig, N. E., M. T. Mellon, K. A. Kretke, and R. E. Arvidson (2005), Global thermal inertia and surface properties of Mars from the MGS mapping mission, *Icarus*, *173*, 325–341.

Schorghofer, N. (2007), Dynamics of Ice Ages on Mars, *Nature*, *449*, 192–195.

Schorghofer, N., and O. Aharonson (2005), Stability and exchange of subsurface ice on Mars, *J. Geophys. Res.*, *110*, E05003, doi:10.1029/2004JE002350.

Sizemore, H. G., and M. T. Mellon (2006), Effects of soil heterogeneity on martian ground-ice stability and orbital estimates of ice table depth, *Icarus*, *185*, 358–369.

Smith, M. D. (2004), Interannual variability in TES atmospheric observations of Mars during 1999-2003, *Icarus*, *167*, 148–165.

Smith, M. D., J. C. Pearl, B. J. Conrath, and P. R. Christensen (2000), Mars Global Surveyor Thermal Emission Spectrometer (TES) observations of dust opacity during aerobraking and science phasing, *J. Geophys. Res.*, *105*, 9539–9552.

Titus, T. N., and T. H. Prettyman (2007), Thermal inertia characterization of the proposed Phoenix landing sites, *Lunar Planet. Sci.*, *38*, 2088.

Titus, T. N., H. H. Kieffer, and P. R. Christensen (2003), Exposed water ice discovered near the south pole of Mars, *Science*, *299*, 1048–1051.

Vasavada, A. R., J.-P. Williams, D. A. Paige, K. E. Herkenhoff, N. T. Bridges, R. Greeley, B. C. Murray, D. S. Bass, and K. S. McBride (2000), Surface properties of Mars' polar layer deposits and polar landing sites, *J. Geophys. Res.*, *105*, 6961–6970.

Wolff, M. J., and R. T. Clancy (2003), Constraints on the size of Martian aerosols from Thermal Emission Spectrometer observations, *J. Geophys. Res.*, *108*, 5097, doi:10.1029/2003JE002057.

Zent, A. P., F. P. Fanale, and J. R. Salvail (1986), Distribution and state of H2O in the high-latitude shallow subsurface of Mars, *Icarus*, *67*, 19–36.

———————

J. L. Bandfield, Department of Earth and Space Sciences, University of Washington, Seattle, WA 98195-1310, USA. (joshband@u.washington.edu)

W. C. Feldman, Planetary Science Institute, 1700 E. Ft. Lowell, Suite 106, Tucson, AZ 85719-2395, USA.